Multi-axial electro-mechanical testing methodology for highly stretchable freestanding micron-sized structures

Shafqat, S.; Savov, A.M.; Joshi, S.; Dekker, R.; Geers, M.G.D.; Hoefnagels, J.P.M.

DOI
10.1088/1361-6439/ab748f

Publication date
2020

Document Version
Final published version

Published in
Journal of Micromechanics and Microengineering

Citation (APA)
Shafqat, S., Savov, A. M., Joshi, S., Dekker, R., Geers, M. G. D., & Hoefnagels, J. P. M. (2020). Multi-axial electro-mechanical testing methodology for highly stretchable freestanding micron-sized structures. *Journal of Micromechanics and Microengineering*, *30*(5), 1-17. Article 055002. https://doi.org/10.1088/1361-6439/ab748f

Journal of Micromechanics and Microengineering

PAPER

Multi-axial electro-mechanical testing methodology for highly stretchable freestanding micron-sized structures

To cite this article: S Shafqat *et al* 2020 *J. Micromech. Microeng.* **30** 055002

IOP Publishing Journal of Micromechanics and Microengineering
J. Micromech. Microeng. **30** (2020) 055002 (16pp) https://doi.org/10.1088/1361-6439/ab748f

Multi-axial electro-mechanical testing methodology for highly stretchable freestanding micron-sized structures

S Shafqat[1], A M Savov[2,3], S Joshi[2,3], R Dekker[2,3], M G D Geers[1] and J P M Hoefnagels[1]

[1] Department of Mechanical Engineering Eindhoven University of Technology, Eindhoven, The Netherlands
[2] Faculty of Electrical Engineering, Mathematics & Computer Science Delft University of Technology, Delft, The Netherlands
[3] Philips Research, Eindhoven, The Netherlands

E-mail: J.P.M.Hoefnagels@tue.nl and s.shafqat@live.com

Received 19 September 2019, revised 14 January 2020
Accepted for publication 10 February 2020
Published 19 March 2020

Abstract

Recent advances in MEMS technology have brought forward a new class of high-density stretchable/flexible electronics as well as large displacement MEMS devices. The in-situ electro-mechanical characterization of such devices is challenging since it requires: (i) highly delicate sample handling, (ii) controlled application of large (hundreds of μm) multi-axial displacements to mimic service conditions, (iii) integrated electrical testing and (iv) fast actuation for cyclic testing. Techniques already developed for small-scale testing in literature fall short to meet the combined set of requirements. To this end, a characterization methodology that fulfills all these requirements is developed and presented here. The technique is based on a piezo-driven micro-tensile stage, which provides large multi-axial displacements with high resolution and fast actuation (4000 μm/s). This is combined with a method for sample microfabrication on a test-chip to warrant delicate sample handling. Proof-of-principle experiments are shown for multi-axial mechanical characterization, electrical characterization and high cycle fatigue testing of micron-sized highly stretchable interconnects. Experiments are conducted under in-situ microscopic observation using optical microscopy, scanning electron microscopy, and high-resolution profilometry. The generic platform proposed here can be used for other problems where similar requirements are faced, e.g. other miniaturized, large displacement electro-mechanical applications that are currently being developed.

Keywords: micromechanical testing, in-situ microscopy, multi-axial loading, stretchable electronics, MEMS

(Some figures may appear in colour only in the online journal)

1. Introduction

By imparting flexibility and stretchability to intrinsically stiff and brittle (micro)electronics, numerous novel breakthrough applications have been reported. The diverse applications of stretchable electronics (SE) include smart health monitoring body patches [1–3], bio-mimicking wide-angle cameras (detectors) [4], and conformal neural implants [5], to name a few.

A typical (hybrid) approach to realize SE devices consists of placing an array of application-specific integrated circuit (ASIC) islands on an elastomer substrate, whereby the islands are electrically connected by metal, stretchable interconnects typically embedded in the elastomer substrate [6]. For many applications, especially detector arrays [7], increasing the (currently low) density of the ASIC islands to match the density of conventional microelectronics is strongly required for improved device performance. To this end, these interconnects

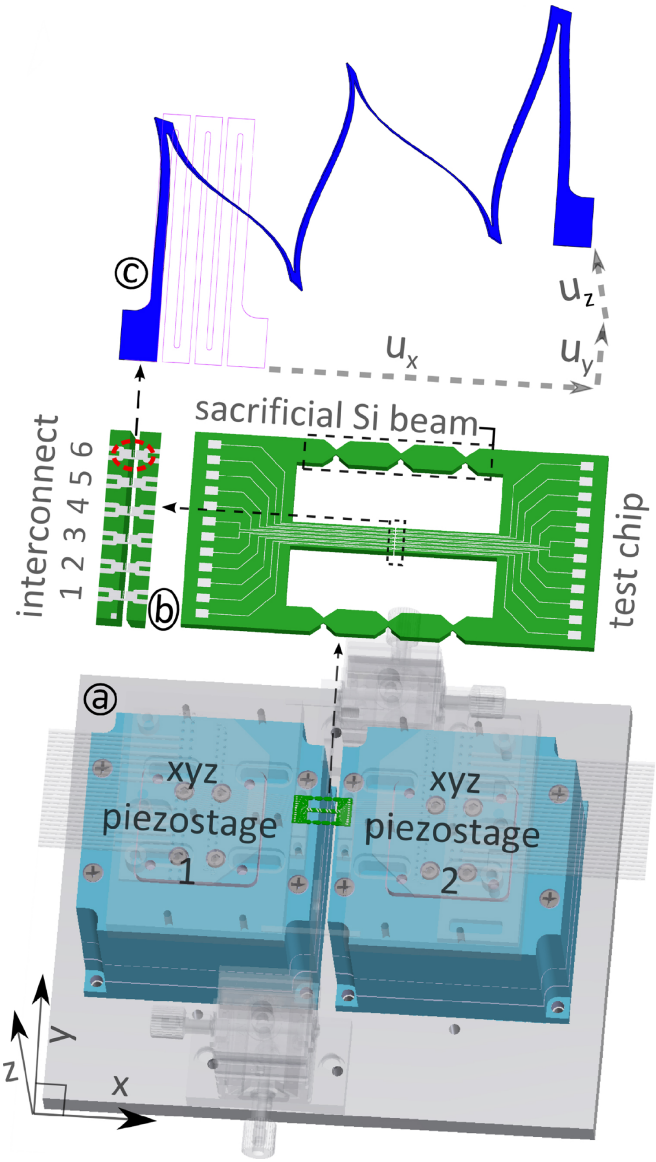

Figure 1. Configuration of the multi-axial tensile stage, based on two piezoelectric stages (a). (b) Zoom-in of the test-chip with 6 samples. (c) The applied multi-axial displacement is illustrated in the (simulated) deformation of one of the 6 interconnects.

need to be miniaturized (with decreased footprint area), which entails an even larger interconnect stretchability to preserve the overall stretchability of the device [8]. Furthermore, in most applications, the interconnects experience in-plane and out-of-plane shear on top of the uniaxial stretch.

To achieve ultra-stretchability, interconnects that are suspended freely between the connecting ASIC islands (i.e. not embedded in the substrate) have been introduced [8–10]. Furthermore, employing standard microfabrication recipes for processing the interconnects allows their miniaturization to the micron scale [8, 11] and beyond, while providing straightforward integration with ASIC island fabrication.

Electro-mechanical characterization of such ultra-stretchable interconnects, which are the critical components in such systems, proves to be challenging, since it requires: (i) multi-axial actuation to mimic real service conditions; (ii) large displacement actuation in the range of 100 s of microns, due to their ultra-stretchable nature; (iii) delicate sample handling, since undesired forces or vibrations during processing and handling can easily result in thousands of percentages of (unintentional) stretching that may damage the interconnects; (iv) integrated electrical monitoring, which can be challenging since conventional bulky probe stations suitable for on-wafer testing need to be integrating with the tensile stage for continuous monitoring; (v) fast actuation for low-cycle and high-cycle fatigue testing to ensure reliability and lifetime requirements, especially for medical devices.

Numerous novel small-scale testing techniques have been developed over the last couple of decades with rapid developments in MEMS technology, notably on-chip testing techniques [12, 13]. While these techniques adequately tackle some of the challenges listed above, e.g. delicate sample handling, with the sample being co-fabricated in a test device, they fall short to meet other challenges, e.g. high displacement actuation [14]. This is mainly due to the fact that these methodologies have been developed for material testing

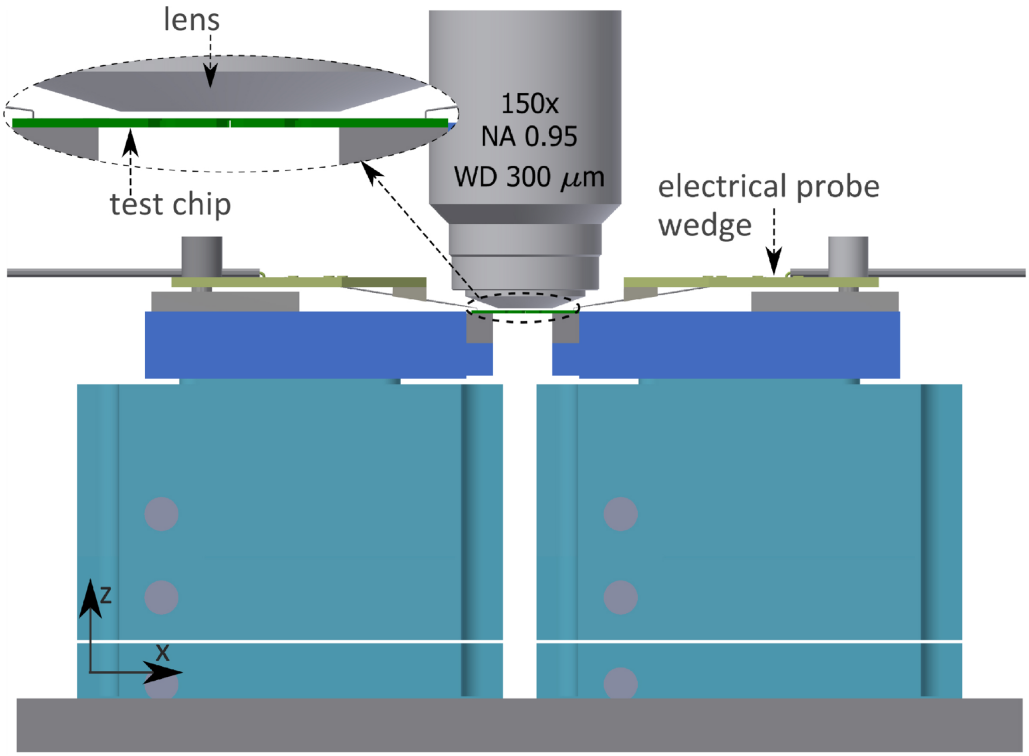

Figure 2. Illustration of the flat-top design of the stage to enable working with high-resolution lens (150x, 0.95 NA) with a working distance of only 300 μm.

(requiring relatively small strains to failure) and not for testing highly stretchable MEMS structures. The latter have emerged only recently with the advent of highly stretchable and large displacement micro-actuators, e.g. for optical scanning applications [15]. Similarly, at the larger scales, various techniques exist to apply complex, multi-axial deformation [16–18], which however cannot be downscaled to micromechanical tests, especially when both an out-of-plane displacement and in-plane displacements need to be imposed. Therefore, in this paper, a new experimental methodology tackling the combined challenges of multi-axial loading, large displacement actuation, delicate sample handling, integrated electrical testing and fast actuation is presented. The methodology consists of a miniaturized, fast actuation, multi-axial tensile stage with integrated electrical probing, along with a test-chip designed to ensure delicate handling of the samples at each stage from fabrication to testing.

2. Setup and test-chip design

Key aspects of the design of the setup and the test-chip are elaborated below.

2.1. Actuation

The actuation of the miniaturized loading stage is based on two high-resolution piezoelectric nanopositioning stages (see figure 1). The vacuum compatible nanopositioning stages (MCL Nano-3D200) each have three (translations) degrees of freedom (along x, y and z axes), enabled by the assembled stack of three stages, specified by the manufacturer to have a resolution of 1 nm (which is established technology for piezoelectric flexure guided nanopositioning stages [19, 20]) and a travel range of 200 μm. The nanopositioning stages are equipped with internal displacement sensors and a control loop to eliminate the creep/drift effects arising from hysteresis in the piezo actuators, for stable actuation even on long time scales. Furthermore, the piezo actuators offer a fast response time, which is needed for (high-cycle) fatigue testing. Combined, the two nanopositioning stages provide a sample actuation range of 400 μm along all three axes, enabling complex multi-axial loading.

2.2. Clamping

The setup has been designed for in-situ, high-resolution Scanning Electron Microscopy (SEM) as well as optical microscopy testing. High-resolution optical microscopy necessitates small working distances, e.g. a 150x lens with 0.95 Numerical Aperture (NA) typically has a working distance of 300 μm. Furthermore, it should be possible to actuate the samples in x, y and z axes. Lastly, the test-chip on which the samples have been processed (figure 1) needs to be clamped rigidly enough, such that the interconnects would not be pre-loaded when a mechanical force is applied to break the sacrificial Si beams (shown in figure 1 and explained later). These requirements put a constraint on the type of sample clamping mechanism that can be used. Typical clamping techniques used in micromechanical tensile testing include, using conventional mechanical screw grips [21], electrostatic clamping [22], pin-in-hole locking [23, 24] and (UV-curable) adhesive clamping

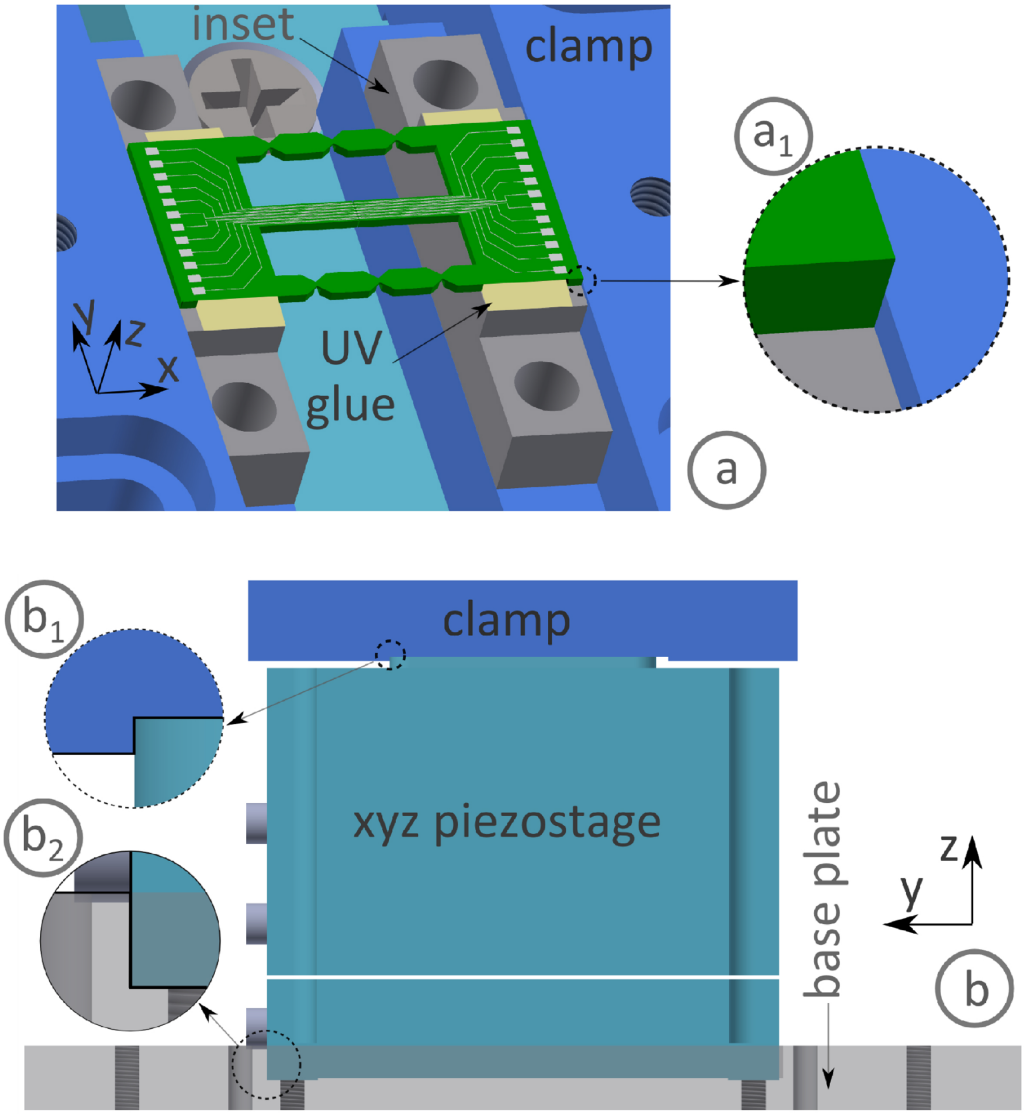

Figure 3. Alignment of the tensile stage components with respect to each other and of the test-chip with respect to the tensile stage, with: (a) test-chip placed on the insets (in grey) and pushed against the corresponding face of the clamp (in blue), (b) vertical face at the bottom of a clamp, pushed against the corresponding vertical face of island protruding out of the piezo stage and (c) the piezoelectric stages pushed against the vertical face of the base plate cavity to align both piezo-stages with respect to each other.

[25], etc. The three requirements stated earlier are most easily met by using a low contraction UV-curable glue applied to the side faces of the test-chip resting on top of the inset faces which have earlier been leveled in height under a profilometer (see figures 2 and 3). Using a (UV-curable) glue allows for the top surface of the test-chip to be free. Furthermore, the test-chip is fully clamped (along all axes), making it possible to apply a force on the sacrificial Si beams as well as subsequently loading the interconnects along x, y, and z axes.

2.3. Alignment

An important aspect to consider in any mechanical test is the proper alignment of the sample with respect to the loading axes to avoid any spurious loading, as elaborated in detail by Saif *et al* [26, 27] in the context of micromechanical testing. This is ensured here by first aligning the test-chip, containing the freestanding interconnects (figure 3), with the clamps. The test-chip is a rectangular platform processed in a 150 mm Si wafer and formed by etching through the wafer thickness. The test-chip consists of two Si islands, for clamping, each supporting the freestanding interconnects at the opposite ends. Sacrificial Si beams are processed into the test-chip to keep the two islands rigid during processing, handling, and test-chip clamping. Microfabrication makes it possible to perfectly align the interconnects with the test-chip itself. Etched (flat) faces of the test-chip provide ideal features to align the test-chip with respect to the clamp. The right (or alternatively left) edge face of the test-chip is positioned against the corresponding (finely milled) vertical edge face of the corresponding clamp to align the samples with respect to the clamp (figure 3(a)). The clamps in turn are aligned with the corresponding loading axes (of the actuators) by placing the (finely milled) vertical edge face of a step machined at the bottom of

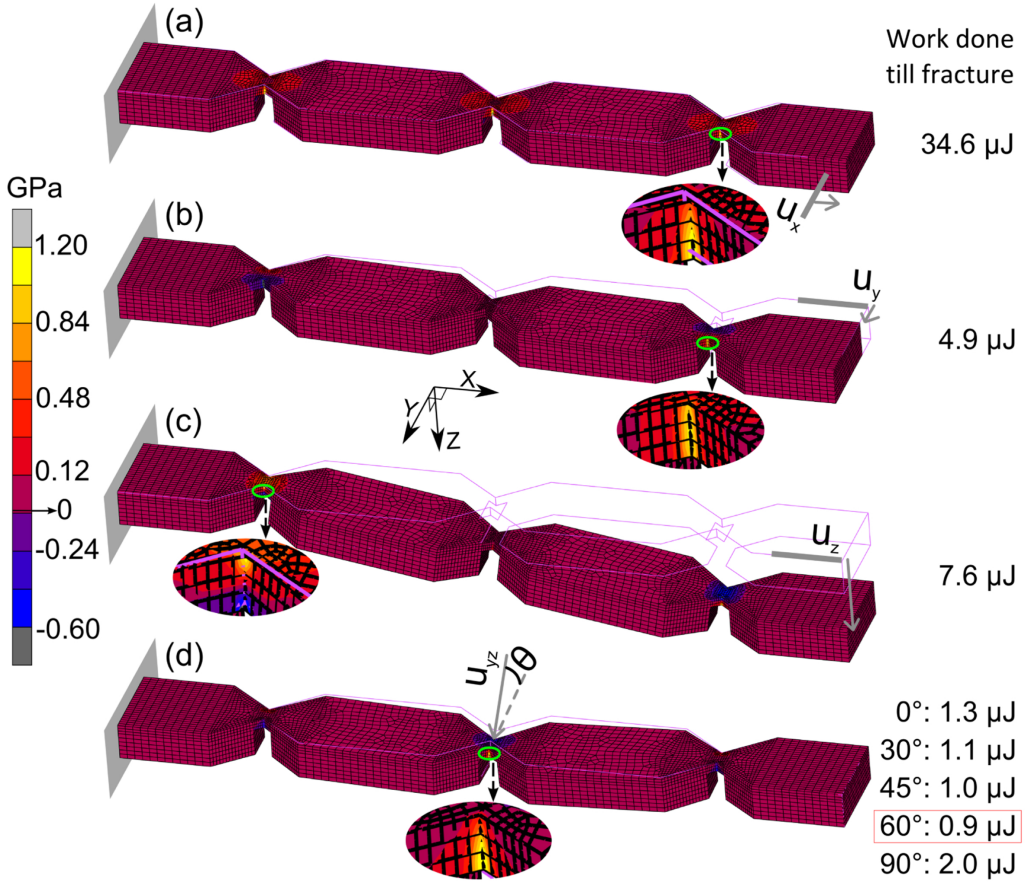

Figure 4. FE simulation to identify the smallest energy to fracture the sacrificial Si beams. (a) Tensile loading along the *x*-axis, (b) in-plane shear loading along the *y*-axis, (c) out-of-plane shear loading along the *z*-axis and (d) point load applied at the central notch at angle θ in the yz plane. The corresponding work done by the applied force/displacement until the fracture stress of 1.2 GPa is reached is displayed to the right of each sub-figure. Note that the deformation has been magnified by a factor of 10 in each sub-figure for visualization.

the clamp against the vertical face of stacked z-stage protruding out from the top of the nanopositioning stage (figure 3(b_1)). Since the nanopositioning stage was machined using electrical discharge machining (by the manufacturer) it provides low-roughness, flat faces appropriate for alignment purposes. Finally, the two nanopositioning stages (and hence the corresponding loading axes) are aligned with each other by positioning and fixing the vertical edge faces of the stages against the vertical edge face of the placement cavity milled into the base plate (figure 3(b_2)). This results in complete alignment of the whole setup and hence the alignment of the interconnect samples with respect to the loading axes.

2.4. Test-chip design for delicate sample handling and testing

After clamping, to start loading the interconnect samples, the sacrificial Si beams (figure 1(b)), processed to keep the two Si islands fixed with respect to each other, need to be broken. The sacrificial Si beams have been designed on the basis of prior Finite Element (FE) simulations to render a high in-plane and out-of-plane stiffness to the test-chip, preventing forces arising from processing, handling, or clamping to be transferred to the interconnect samples. Whereas, after the silicon islands of the test-chip have been clamped, it is desired that only a small force is needed to break the sacrificial Si beams, to make sure that the loads that are transferred to the interconnects remain negligible. To this end, the sacrificial Si beams contain sharp notches (see figure 4) created by thinning the sacrificial Si beams through thickness as well as the in-plane direction, to trigger localized high stresses and initiating local fracture. Due to the brittle and single crystalline nature of the test-chip material the local crack(s) propagate easily all the way through the cross-section of the sacrificial Si beams. Here the beam width has been aligned along the <100> crystalline direction of the Si wafer. Using three notches in the sacrificial Si beam significantly reduces the required load for bending, while more than three notches would only negatively affect the test-chip stiffness during handling and clamping. Exploiting FE simulations, various deformation modes of the beam are explored to identify the lowest energy to fracture mode. If the test-chip is deformed as a whole, e.g. in tension (see figure 4(a)), or even in-plane (see figure 4(b)), or out-of-plane shear (see figure 4(c)), a high amount of energy would be required to reach the fracture stress of Si (~1.2 GPa [28]) in the notches. If, on the contrary, a local point force is applied downwards (along the *z*-axis), on the central notch of a sacrificial Si beam it requires only 2 μJ to reach fracture. This value is even lower if the force is applied at an angle of 60° with respect to the notch width.

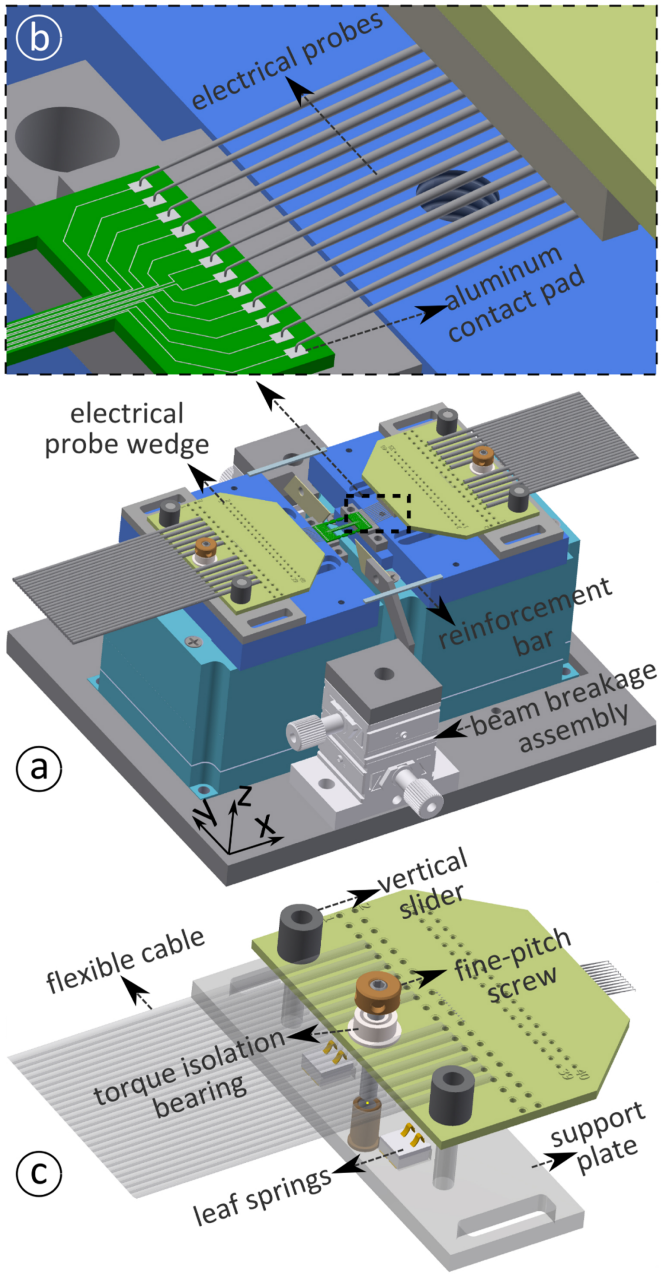

Figure 5. Illustration of: (a) electrical resistance probe assembly integrated with the piezo electric stage, (b) a magnified view of the the electrical probes in contact with the Al contact pads on the test-chip, and (c) details of the electrical probe assembly components.

To apply this localized force, a miniature load assembly is made, with a razor a blade edge at an angle of 60° with respect to the notch width attached to a miniature linear x, y stage (DT12XY stage by Thorlabs) as shown in figure 5(a). The razor blade edge is first aligned with the central notch and then carefully inserted into the notch to conveniently fracture it in a well-controlled manner.

2.5. Electrical probing for simultaneous electro-mechanical testing

Additional to the mechanical characterization, the electrical characterization of such interconnect structures (or other MEMS structures), i.e. the evolution of electrical resistance with deformation, is essential. This is particularly pertinent here since a high interconnect stretch is required and a significant change in electrical characteristics with large deformation can affect the performance of the SE device. To this end, an approach for in-situ electrical characterization during mechanical loading is developed. This allows for less cumbersome testing compared to ex-situ testing using probing stations, often used in the semiconductor industry for intermittent quasi-static testing. Furthermore, continuous electrical monitoring allows to detect interconnect failure during fatigue testing as shown below. The approach adopted here is to have miniaturized custom built (12 needles) wedge probes directly mounted on the clamps (see figure 5), such that there is no relative movement between the probe needles and the test-chip

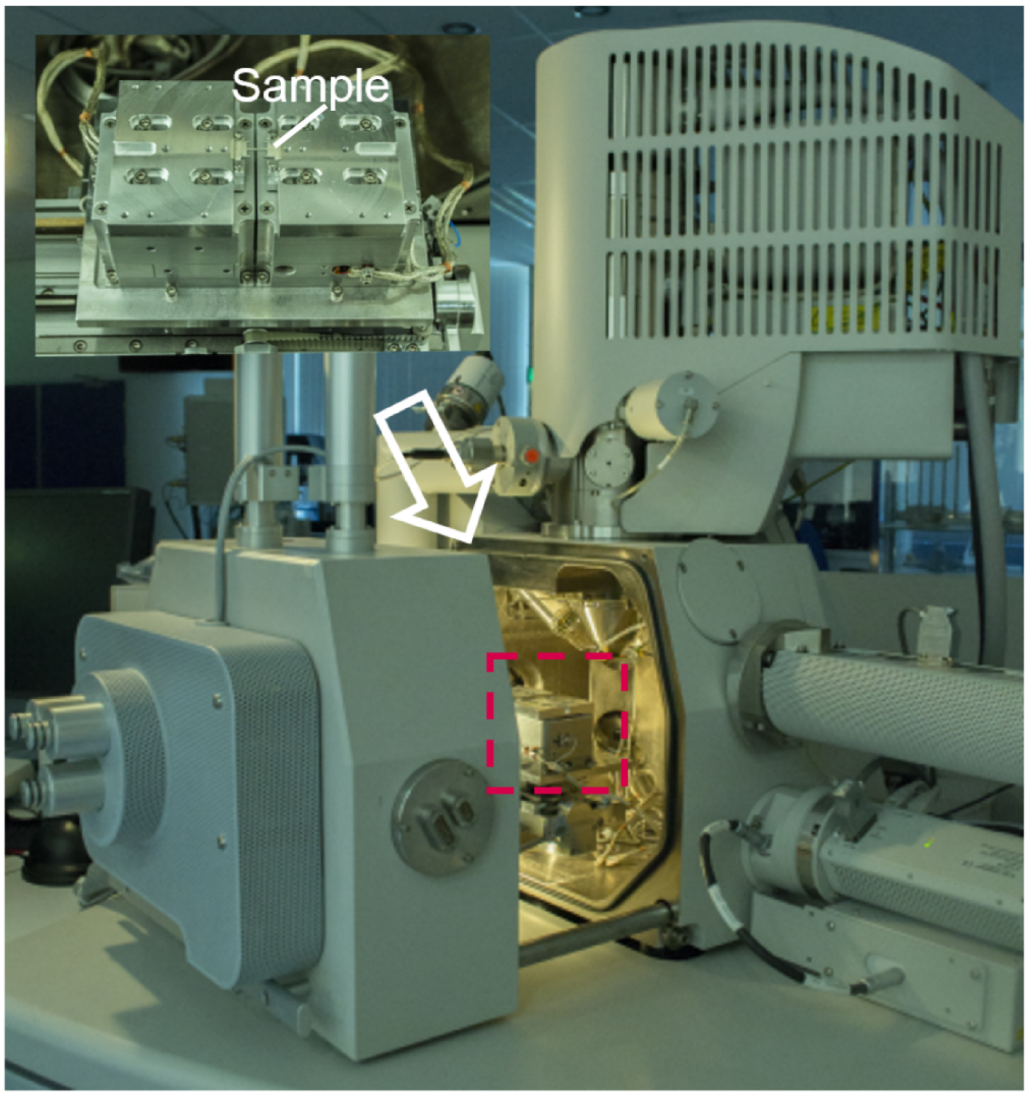

Figure 6. The tensile stage placed inside the FEI Quanta 600 ESEM. The high-vacuum compatible tensile stage can be tilted ($+5^{\circ}$ to -75°) with the SEM sample stage.

during tensile testing. The probe wedges are mounted on the clamps through a miniaturized custom-built vertical manipulator. The wedge can be moved vertically with the help of two sleeves attached to each wedge, sliding along lubricated vertical shafts attached to a bottom plate, which itself is screwed to the clamp. The vertical displacement is controlled with the help of a screw of an extremely fine pitch of 200 μm (by Thorlabs), providing a high resolution of ~6 μm (assuming 10° minimum rotation) (see figure 5(c)). A miniature bearing is glued to the bottom side of the manipulator screw head to isolate the torque applied on the screw from being applied to the probe wedge. Leaf springs attached to the bottom plate ensure that the wedge and consequently the probe needles can be moved down in a well-controlled fashion and provide a vertical force to retract the wedge after the test. On the test-chip, two wires from each per interconnect fan out to a total of 12 contact pads, on either side of the test-chip, to allow four-point probe electrical resistance measurements (see figure 5(b)). The electrical measurements and data acquisition are performed using an integrated multimeter and data acquisition system (Keithley 2701) with a multiplexer module (Keithley 7700), to be able to measure the resistance of all six interconnects in parallel.

The whole setup is vacuum compatible and designed for high vacuum conditions (up to 10^{-6} mbar), enabling high-resolution in-situ SEM testing. The miniaturized setup can easily fit inside the SEM chamber, even with the possibility to tilt the SEM stage. Furthermore, the flat top design is instrumental for imaging at small working distances for high-resolution imaging. An image of the setup placed inside the chamber of FEI Quanta 600 SEM is shown in figure 6.

3. Experimental methodology

To start a test, first, the test-chip is extracted from the Si processing wafer (figure 7). The test-chips are suspended in the wafer with the help of polyimide tabs (see figure 7(b)), which can be conveniently removed using, e.g. a low-cost CO_2 laser cutter or a razor blade mounted on a manual manipulator. The

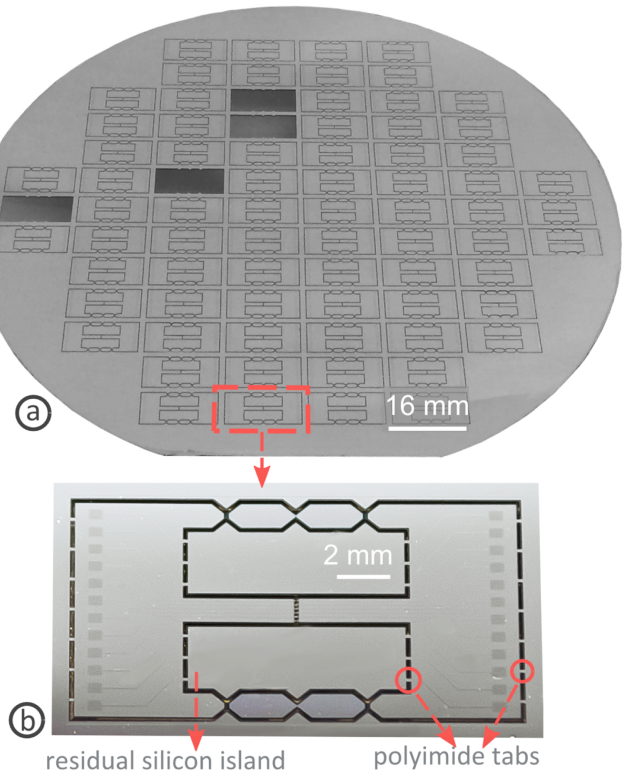

Figure 7. Fabricated test-chips with photographs of: (a) the full 150 mm wafer and (b) a fabricated test-chip suspended in the Si wafer with the help of polyimide (PI) tabs. The residual silicon islands are processed to define the inner geometry of the test-chip without having to etch the full cavities. The thin PI tabs, which can be easily cut, help avoid the need of employing mechanically or thermally aggressive wafer dicing processes

PI tabs help to avoid the use of, e.g. mechanically aggressive saw dicing, which could damage the freestanding interconnects, or the use of an expensive dicing laser [29]. Next, with the help of wafer tweezers the sample is placed on the top surface of the clamp insets. The left (or alternatively right) face of the test-chip is pushed against the corresponding face of the clamp. Subsequently, UV-curable glue is applied on the top and bottom edges of the test-chip while ensuring that the glue does not rise above the top surface of the test-chip, which could impede the use of low working distance lens. Illuminating the glue for 30 mins with a UV lamp sets the glue. Finally, the reinforcement bars (see figure 5(a)) are placed on the clamps on the top and bottom sides and then glued to the clamps by apply air-drying silver paint.

Once the clamping procedure has been completed, the knife-edge of the beam breakage assembly (see figure 5(a)) is heightened to be at the level as the test-chip with the help of adjustment screw and delicately moved with the miniaturized linear stage into the central notch to conveniently break it. Note that as explained earlier, only a minute force is needed to break the sacrificial Si beam. After breaking the notched silicon sacrificial Si beams, the glued temporary reinforcement bars are also removed before the specimen loading can be initiated. This is done by locally applying a few drops of acetone with a syringe to dissolve the dried silver paste. The temporary reinforcement bars are then removed by retracting the sacrificial Si beam breakage assembly, with the slanted edge of the assembly frame, pushing the reinforcement bars backward. Now the loading can be applied to the interconnects. Since six parallel interconnects are processed in each test-chip, six of them can be simultaneously tested in one experiment. A custom-built LabVIEW interface is used to apply the loading in displacement control, enabling complex loading paths representative of interconnect loads in real devices.

4. Proof of principle experiments

A typical uniaxial tensile loading test is shown in figure 8. Initially, the loading is applied in small increments to study the onset of buckling (see figure 8(d)). At each loading step, the interconnect is unloaded to the initial configuration to compare the shape of the interconnect with the initial shape, in order to determine the onset of plasticity in parts of the interconnect. Beyond the engineering elastic limit (figures 8(e), (f)), which is the point where the interconnect still recovers its original shape, the interconnect is incrementally stretched further beyond the elastic limit, reaching a high axial displacement, until finally fracture occurs (figure 8(g)).

For such structures, besides uniaxial stretching, multi-axial characterization is equally important, i.e. application of in-plane as well as out-of-plane shear loading to mimic the interconnect loading in real service conditions. Similar to tensile loading, for in-plane shear loading large displacements can be conveniently applied with the piezoelectric stages since the resolution and displacement range along all three axes is

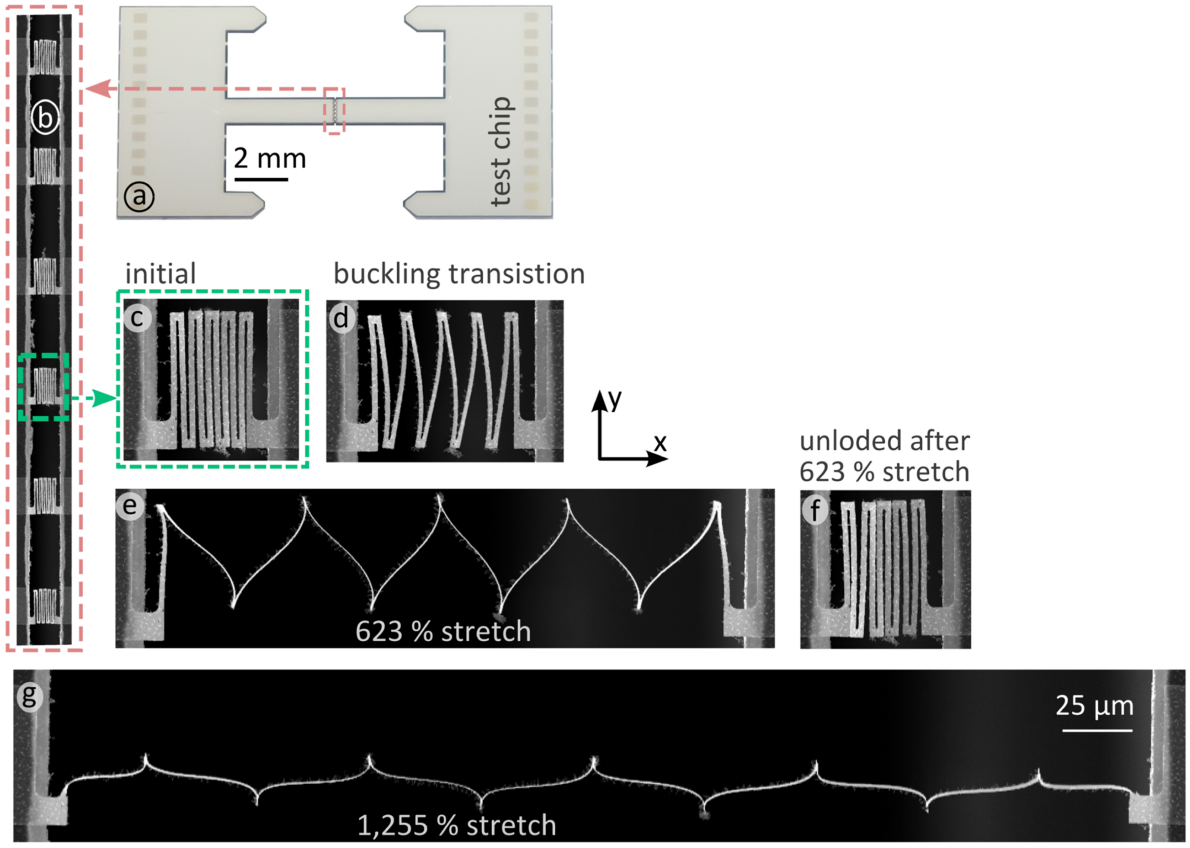

Figure 8. Proof-of-principle uniaxial tensile test results with the interconnects stretched in the in-plane x-direction. (a) Test-chip with broken sacrificial Si beams, ready to be actuated, (b) SEM micrograph of all 6 parallel interconnects in the test-chip, (c) a magnified view of the initial stage of interconnect no 4, imaged throughout the loading, (d) interconnect transitioning from a planar configuration to a 90° rotated out-of-plane configuration after application of a minute displacement, (e) interconnect stretched to its maximum elastic stretch of 623%, (d) unloaded configuration after the maximum elastic stretch and (g) plastic stretch of 1,255%.

identical. As in the case of the uniaxial tensile loading, initially, small displacements steps in increments of 1 μm are applied to study the onset of buckling, while later on larger steps may be applied with subsequent unloading of the sample to its original position to study the onset of plasticity, as shown in figure 9.

A unique feature compared to other small scale testing setups is that out-of-plane (shear) loading based characterization can also be easily performed. In order to visualize the out-of-plane displacement better, the setup is tilted by 5° with respect to the electron beam with the help of the SEM tilt stage. Since for these interconnects, there is no buckling transition occurring in the out-of-plane opening mode, the initial displacements are not chosen to be small as in the previous two tests.

The change in the electrical resistance of the samples with applied deformation is studied with the help of the four-point probe resistance measurement assembly described earlier. The electrical characterization during mechanical loading can be performed for any type of multi-axial (xyz) loading path. To start the test, after fixating the sample and before removing the sacrificial Si beam, the electrical probes are aligned with the contact pads under an optical microscope (figure 11) and constrained in the in-plane directions with the help of fixation screws. The probe tip diameter is 50 μm, while the contact pad pitch, i.e. the center to center distance between two adjacent pads is 640 μm, which is large enough to allow the in-plane alignment between the probes and pads manually without an additional XY translational stage. Once fixed, the probe wedge is moved downwards by rotating the ultra-fine threaded screw, while visualizing the probes through the microscope. Contact between the probes and the pads manifests itself through an increased reaction moment on the screw, which is simultaneously verified through the microscope. Upon contact, the probe wedge is moved further down by ~25 μm, i.e. a quarter rotation of the screw, to ensure that all probes make good contact with the contact pads. The titanium probes allow for a 100 μm elastic deflection, i.e. the deflection.

In order to make electrical contact, the insulating native oxide film on the Al contact pads is broken by mechanical force applied by the probe needles and the electrical connection is maintained by the continuous current applied during the electrical resistance measurement as discussed in [30–32]. A good electrical connection is verified before mechanical testing by stabilizing the resistance (for a few minutes) until transient effects have passed. Finally, the cables connecting the probe card to the multimeter are chosen to be very compliant, in order to not pose any asymmetric load to the relatively

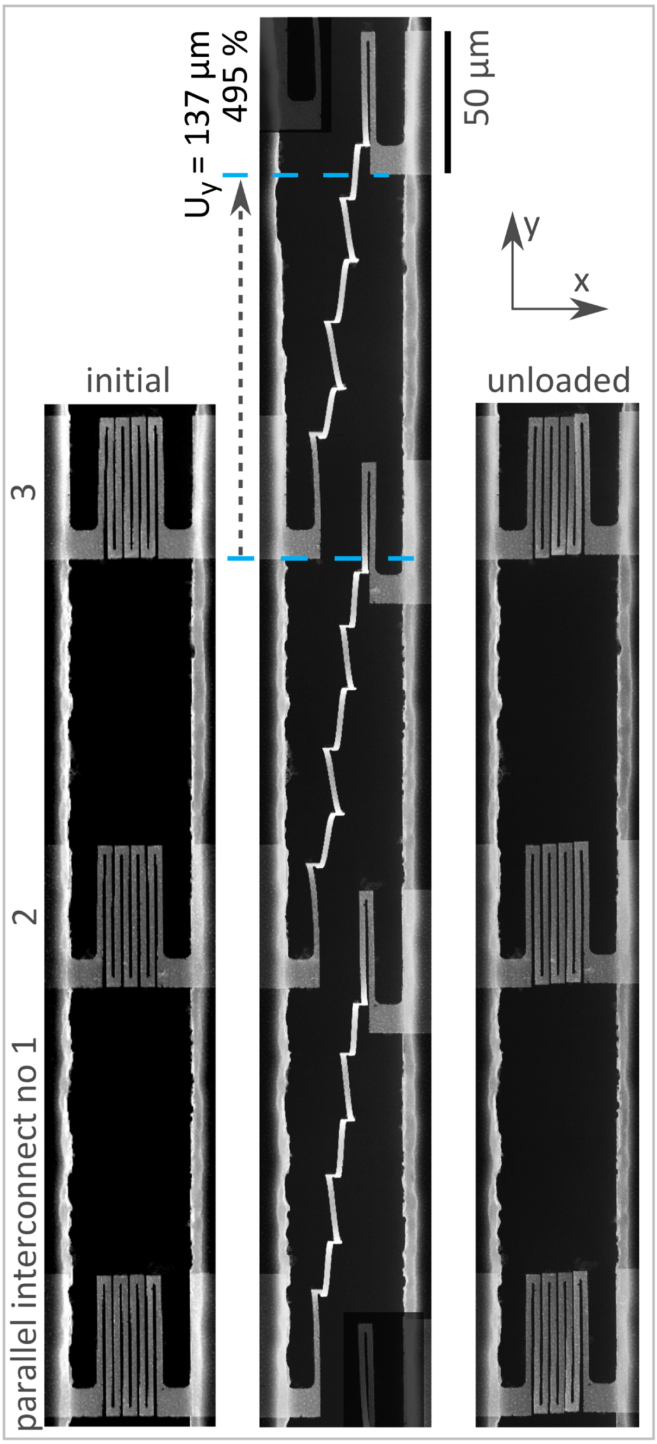

Figure 9. Proof-of-principle test showing 3 of the 6 parallel interconnects loaded in in-plane (xy) shear with: (left) the initial configuration to, (middle) loaded to maximum elastic in-plane shear of 495% and, (right) being unloaded after the maximum elastic stretch.

compliant flexure stages. In order to measure all (six) interconnect resistances in parallel, the probe wedge cables are connected to the multimeter through a Keithley 7700 multiplexer module, capable of supporting ten four-point probe resistance measurements. At each loading stage (multiple) resistance measurements are acquired for each of the six interconnects, as shown in figure 12. The experiments were performed in temperature-controlled conditions with a maximum variation of 1 $^{\circ}$C, to reduce the influence of ambient temperature on the resistivity.

For application purposes, it is important to characterize the repeated usage and fatigue behavior of stretchable interconnects and MEMS devices considering the cyclic loading in their applications. The actuation stages, with the fast reacting piezo elements and their flexure mechanism based design enable convenient fatigue testing, which is considerably more

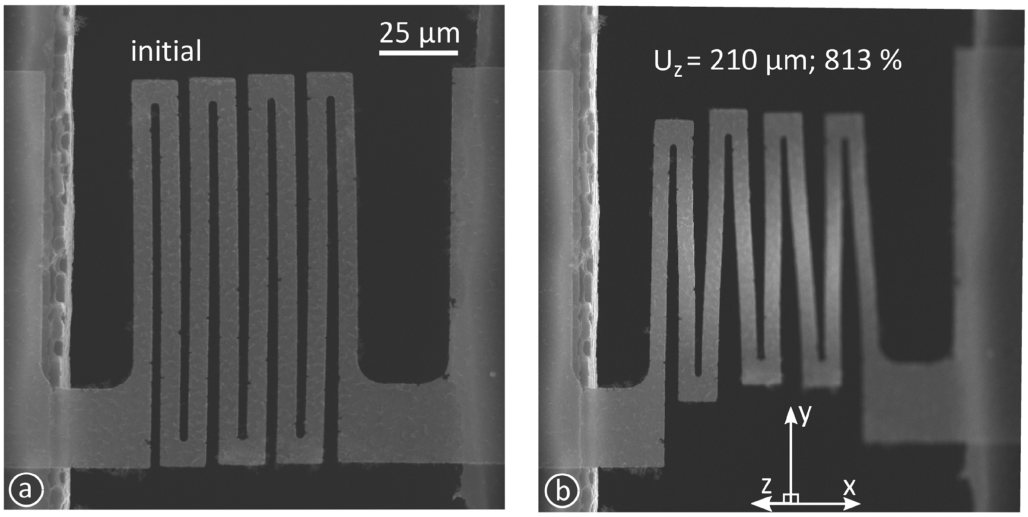

Figure 10. Proof-of-principle tensile test results with an interconnect loaded in the out-of-plane z-direction from (a) the initial configuration to (b) a stretch of 813%. To better visualize the out-of-plane displacement the SEM stage has been tilted by 5°.

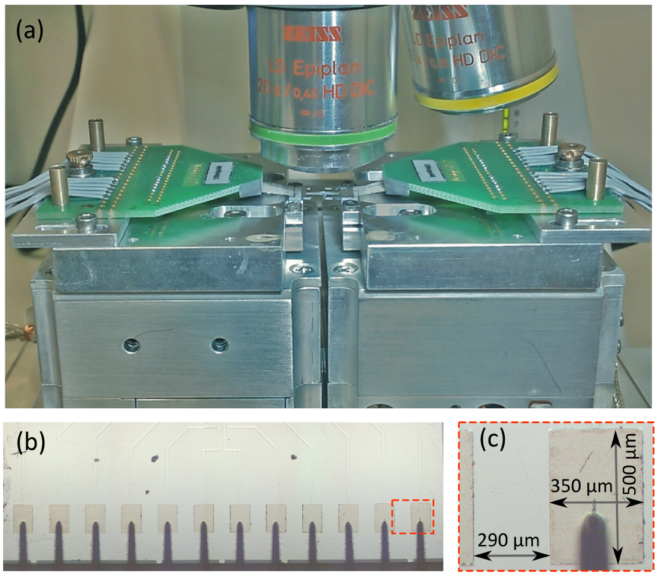

Figure 11. Illustration of the 4-point probe electrical resistance measurement setup, with (a) tensile stage with integrated testing probes, under optical microscope, (b) the probe tips aligned on top of their corresponding contact pads of the test-chip and (c) a magnified view of a probe tip in contact with the corresponding contact pad.

difficult with the geared, motorized systems [33]. In order to achieve the maximum actuation frequency (for feasible testing durations), a predetermined square waveform (see figure 13) is sent to the controller through the LabVIEW GUI, with which a maximum actuation frequency of 10 Hz is achieved. While this frequency is large enough for fatigue testing, the inertia effects in the compliant sample structures, such as the highly stretchable interconnects are still negligible. The electrical resistance of the interconnects is monitored as well during the cyclic loading, with open-circuit resistance serving as a convenient criterion to detect interconnect failure. More importantly, a systematic resistance change occurs due to plasticity and/or defect evolution during cyclic loading. For the results displayed in figure 13, optical microscopy images are captured every million cycles to complement the electrical resistance results. The results shown here are for uniaxial tensile loading of the 100 μm tall interconnects stretched up to 1000% (half of the plastic stretch value). All interconnects survive up to 10 million cycles without failure. The variation of the interconnect resistance lies within a range of 1%, which is mainly attributed to variations of the ambient temperature and a systematic increase or decrease of the resistance cannot be observed.

Due to the sub-micron characteristic length (thickness in this case), the material properties of the interconnect and similar microfabricated samples can greatly vary from bulk properties as a result of mechanical size-effect being active and consequently the material properties cannot be

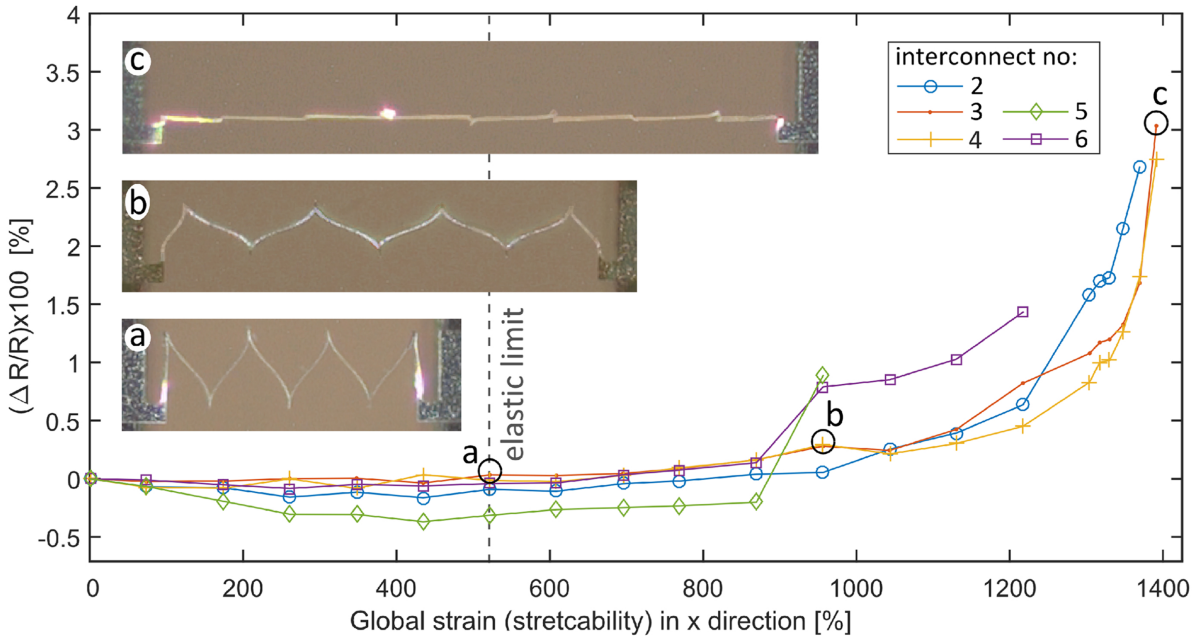

Figure 12. The evolution of the electrical resistance with applied stretch, displaying only a small variation till ~1000% stretch (beyond the elastic limit) and a steeper increase to a maximum of ~3% before interconnect failure. Note that interconnect 1 was missing from the beginning of the test for this test-chip, reflecting the fact that the yield was not optimal of the non-optimized microfabrication process

assumed *a priori* [34]. A material strengthening effect was also observed in the case of uniaxial tensile tests performed on the freestanding interconnects. A qualitative estimation of the strengthening was made by fitting FEM simulations to the experiments [8]. Typically, dedicated test samples with the same sizes and processing conditions are fabricated and tested (e.g. by a tensile test) to characterize the material behavior. In case of the freestanding interconnects another consideration needs to considered, i.e. the size effect might also be dependent on the deformation modes of interconnect, more specifically bending induced strain gradient effects [35]. Therefore, testing on the original sample is highly preferred. A stretching (uniaxial tensile test) on the freestanding interconnect sample to characterize its material behavior however entails force resolution of few nano-Newtons (due to highly compliant structure), along with very delicate sample handling and load transfer functionalities as discussed in [36]. Alternatively, inverse methods such as FEM updating (FEMU) or integrated digital image correlation (IDIC) [37] can be utilized to circumvent some of these complications.

A variation of IDIC which utilizes surface topographical images and termed as integrated digital height correlation (IDHC) [38, 39] was utilized for the sample characterization. A confocal optical profilometer (Sensofar S neox) with a 100x magnification lens having a numerical aperture of 0.9 and working distance 1 mm was used to obtain topographical images. The samples were loading out-of-plane in the z direction with incrementally higher displacement-controlled loads and subsequently unloaded after each load step. Ideally, the topographical images of the interconnects in the out-of-plane loaded condition would be utilized for the IDHC. However, even at relatively small out-of-plane displacements of tens of μm, interconnect beams bend with large gradients and the topography cannot be captured even with a high numerical aperture lens. The topography of the sample in the unloaded configuration could, however, be captured and was recorded after unloading from each incrementally increasing displacement load. With the onset of plasticity, the sample geometry would change in the unloaded configuration as a result of accumulated plasticity and can be quantified by correlating the unloaded (deformed) shape with the original unloaded (undeformed) shape.

To enable DHC on the freestanding interconnect sample, a pattern is needed to be applied as the native pattern was insufficient. A pattern consisting of 300 nm silica nanoparticles was applied the sample using a dried micro-mist technique. Due to the scarcity of the available samples, the pattern could not be optimized and only a sparse pattern (of unclustered nanoparticles) was applied (see figure 14(a)). However, in this case essentially the change in curvature of the interconnect beams as a result of plasticity was required to be captured, for which a few particles over the beam length were deemed sufficient. Furthermore, a global-DHC approach [40] was used here, which reduced the requirement on pattern density due to higher-order continuity. The sample was meshed with isogeometric elements with four elements over the interconnect beam length and one element over the beam width. Non-Uniform Rational B-Splines (NURBS) shape functions were used to capture the displacement fields with second order shape functions in the beam length direction and zeroth order shape function on the beam width direction. The in-plane and out-of-plane displacement fields obtained from the application of DHC are shown in figures 14(b)–(d). As shown in figure 14(e) the image residual has a very low average value with

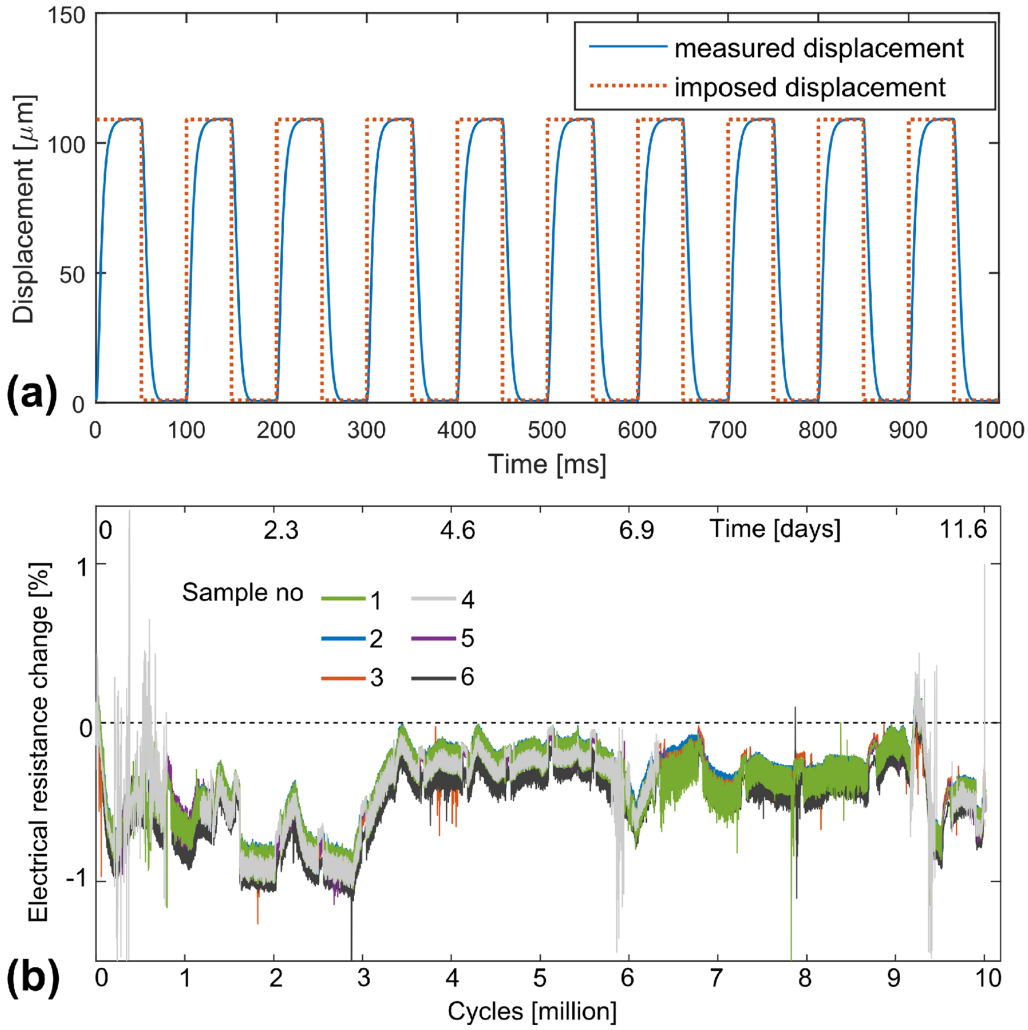

Figure 13. Fatigue test results for interconnects with a height of 100 μm, with (a) the applied displacement waveform (in blue) and the measured displacement (in red) for the piezo-stage at 10 Hz and (b) the measured interconnect electrical resistance change as a function of the applied number of cycles, showing that all six interconnect survive until 10 million cycles at an amplitude of 1000% stretch.

no systematic variations, indicating an accurate correlation. Results form the IDHC are out of scope of this work and are presented in [38]. The experimental characterization procedure mentioned here can be utilized where similar constraints are present, e.g. in the case of freestanding interconnects or MEMS devices.

4.1. Conclusions and recommendations

This paper presented an experimental methodology for electro-mechanical characterization under in-situ microscopic observation of highly stretchable micron-sized structures such as interconnects for stretchable electronics or other MEMS applications where large multi-axial displacements and a high resolution at the micrometer scale matters. The design of a multi-axial test setup is presented, along with sample handling and clamping procedures based on a test-chip platform on which the micron-sized samples are microfabricated. As a proof of principle, in-situ multi-axial tensile test experiments with four-point probe electrical characterization are shown for quasi-static loading and high-cycle fatigue.

The setup is based on two commercially available piezo flexure position stages for actuation, a technology that has matured over the last few decades for nanopositioning systems, providing fast, multi-axial and high-resolution actuation. Typical systems also come with drivers, e.g. for LabVIEW, making it possible to build GUIs with rich and customizable functionality with relative ease. For such piezoceramics based systems, creep, hysteresis and thermal drift are well known issues [41]. Therefore, it is important to use piezo stages with integrated closed-loop control systems. Different displacement sensing options are available for such systems, each with its own advantages and disadvantages [42]. Therefore, when choosing piezo stages for actuation it is important to choose the appropriate sensing solution and verify the performance of the control system based on the particular test of interest, e.g. quasi-static testing, creep testing or high-temperature testing, each with its own set of requirements. Another important aspect to consider is that the piezo stages are relatively compliant when compared with geared-motorized stages due to their flexure based design. Therefore, appropriate measures, such as discussed here, need

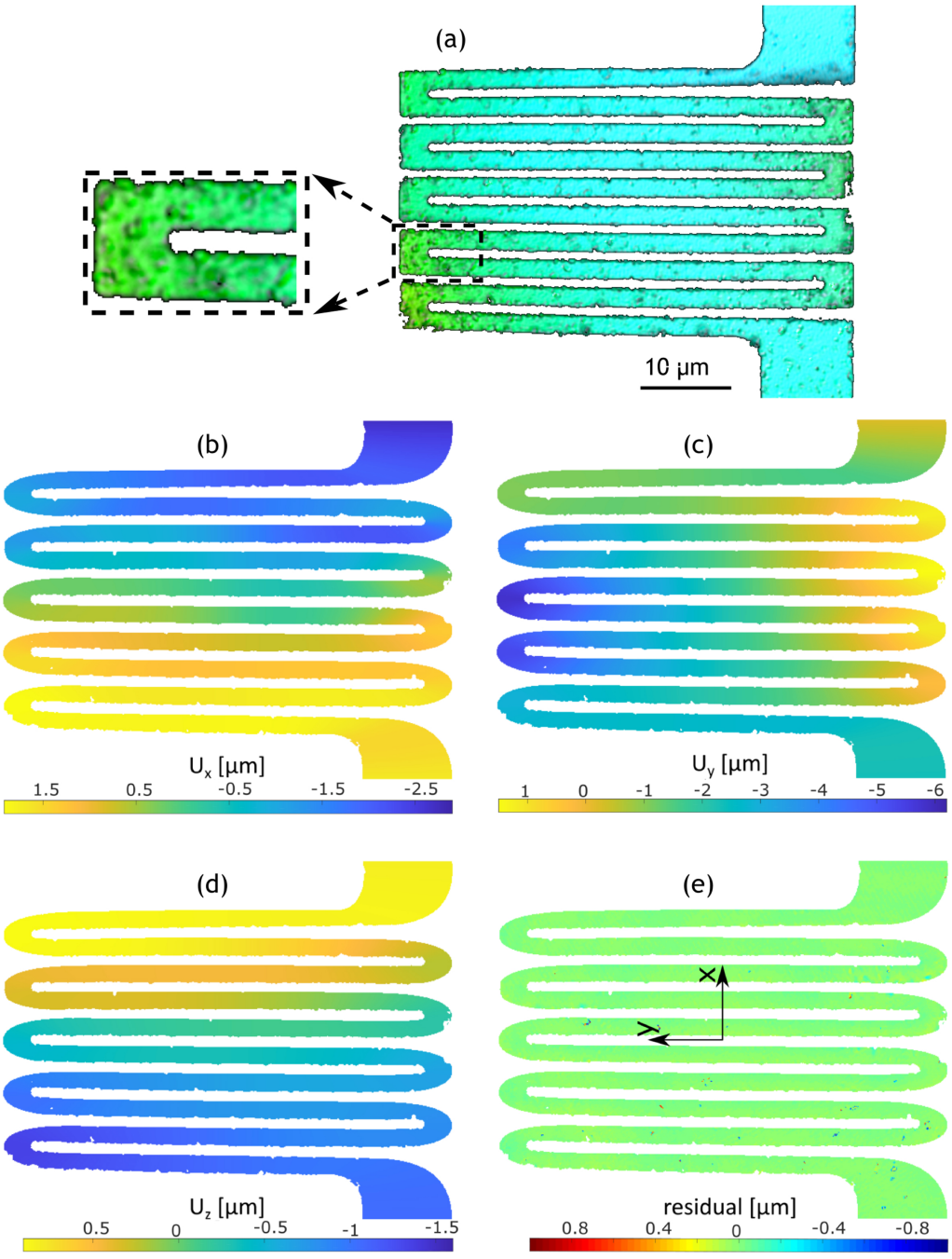

Figure 14. Results from application of digital height correlation (DHC) on the freestanding sample. (a) Topographic image of the test specimen in the undeformed configuration before the test, measured with optical profilometry; the zoom of the corner section shows the nanoparticles that form the topographical contrast used as pattern for DHC (note that the particles are barely visible due the diffraction-limited in-plane optical resolution). (b) In-plane u_x displacement field. (c) In-plane u_y displacement field. (d) Out-of-plane u_z displacement. (e) Image residual field.

to be taken to ensure that the samples are not pre-loaded during the sample clamping procedure. Moreover, typical piezo flexure actuation stages are not designed to handle large loads [41], e.g. the system used here is rated at 10 N by the manufacturer, which is enough for many small-scale testing cases, however, for larger forces a specialized piezo stage or geared systems may be needed instead. For electrical characterization with simultaneous mechanical loading, commercially available customized probe wedges were mounted directly on the clamps with a custom-built miniaturized manipulator as a simple, yet an accurate probing solution. The Si based test-chip on which the samples have been fabricated is obtained by regular microfabrication processing, typically used for the fabrication of MEMS structures. The test-chip design ensures that it is rigid during processing and handling while easily set free by minute mechanical force to start testing. Finally, it is important to note that the testing methodology is not suitable for all

applications, e.g. small-scale material testing which involves relatively small scale gauge displacements to sample failure and thus requiring extremely fine sample handling would require other small scale testing techniques such as ones detailed in [13, 26, 43–45]. The methodology discussed here is, however, meant for small-scale tests where large multi-axial gauge displacements are required for characterization along with electrical probing and fatigue testing, which is a necessity for stretchable electronics interconnects and large displacement MEMS devices.

Acknowledgments

This work was supported by the Vidi funding of J.H. (project number 12966) within the Netherlands Organization for Scientific Research (NWO). The authors would like to acknowledge Lucien Cleven for fabricating the setup, Sandra van de Looij–Kleinendorst for providing the digital height correlation results and Marc van Maris for technical support.

ORCID iD

J P M Hoefnagels https://orcid.org/0000-0001-8359-7575

References

[1] Kim J *et al* 2016 Battery-free, stretchable optoelectronic systems for wireless optical characterization of the skin *Science Advances* **2** e1600418
[2] Son D, *et al* 2014 Multifunctional wearable devices for diagnosis and therapy of movement disorders *Nat. Nanotechnol.* **9** 397–404
[3] Trung T Q and Lee N E 2016 Flexible and stretchable physical sensor integrated platforms for wearable human-activity monitoring and personal healthcare *Adv. Mater.* **28** 4338–72
[4] Song Y M *et al* 2013 Digital cameras with designs inspired by the arthropod eye *Nature* **497** 95–9
[5] Minev I R *et al* 2015 Electronic dura mater for long-term multimodal neural interfaces *Science* **347** 159–63
[6] Someya T 2012 *Stretchable Electronics* (Weinheim, Germany: Wiley-VCH Verlag GmbH & Co.)
[7] Jung I, Xiao J, Malyarchuk V, Lu C, Li M, Liu Z, Yoon J, Huang Y and Rogers J A 2011 Dynamically tunable hemispherical electronic eye camera system with adjustable zoom capability *Proc. Natl Acad. Sci.* **108** 1788–93
[8] Shafqat S, Hoefnagels J, Savov A, Joshi S, Dekker R and Geers M 2017 Ultra-stretchable interconnects for high-density stretchable electronics *Micromachines* **8** 277
[9] Lanzara G, Salowitz N, Guo Z and Chang F K 2010 A spider-web-like highly expandable sensor network for multifunctional materials *Adv. Mater.* **22** 4643–8
[10] Xu S *et al* 2013 Stretchable batteries with self-similar serpentine interconnects and integrated wireless recharging systems *Nat. Commun.* **4** 1543
[11] Hussain A M and Hussain M M 2016 CMOS-technology-enabled flexible and stretchable electronics for internet of everything applications *Adv. Mater.* **28** 4219–49
[12] Colla M S, Amin-Ahmadi B, Idrissi H, Malet L, Godet S, Raskin J P, Schryvers D and Pardoen T 2015 Dislocation–mediated relaxation in nanograined columnar palladium films revealed by on–chip time–resolved HRTEM testing *Nat. Commun.* **6** 1–8 25557273
[13] Zhu Y and Espinosa H D 2005 An electromechanical material testing system for in situ electron microscopy and applications *Proc. Natl Acad. Sci.* **102** 14503–8
[14] Bell D J, Lu T J, Fleck N A and Spearing S M 2005 MEMS actuators and sensors: Observations on their performance and selection for purpose *J. Micromech. Microeng.* **15** 153–64
[15] Choi J, Qiu Z, Rhee C H H, Wang T and Oldham K 2014 A three-degree-of-freedom thin-film PZT-actuated microactuator with large out-of-plane displacement *J. Micromech. Microeng.* **24** 075017
[16] Carpiuc-Prisacari A, Poncelet M, Kazymyrenko K, Leclerc H and Hild F 2017 A complex mixed-mode crack propagation test performed with a 6-axis testing machine and full-field measurements *Eng. Fract. Mech.* **176** 1–22
[17] Cognard J Y, Sohier L and Davies P 2011 A modified Arcan test to analyze the behavior of composites and their assemblies under out-of-plane loadings *Composites* **42** 111–21
[18] Tasan C C, Hoefnagels J P M, Dekkers E C A and Geers M G D 2012 Multi-axial deformation setup for microscopic testing of sheet metal to fracture *Exp. Mech.* **52** 669–78
[19] Yong Y K, Moheimani S O R, Kenton B J and Leang K K 2012 Invited review article: High-speed flexure-guided nanopositioning: Mechanical design and control issues *Rev. Sci. Instrum.* **83** 121101
[20] Ouyang P R, Tjiptoprodjo R C, Zhang W J and Yang G S 2008 Micro-motion devices technology: The state of arts review *The Int. Journal of Advanced Manufacturing Technology* **38** 463–78
[21] Tung S-H, Shih M-H and Kuo J-C 2010 Application of digital image correlation for anisotropic plastic deformation during tension testing *Opt. Lasers Eng.* **48** 636–41 (www.sciencedirect.com/science/article/pii/S0143816609002358)
[22] Tsuchiya T, Tabata O, Sakata J and Taga Y 1998 Specimen size effect on tensile strength of surface-micromachined polycrystalline silicon thin films *J. Microelectromech. Syst.* **7** 106–13
[23] Cheng Y-W, Read D T, David McColskey J and Wright J E 2005 A tensile-testing technique for micrometer-sized free-standing thin films *Thin Solid Films* **484** 426–32 (www.sciencedirect.com/science/article/pii/S0040609005003287)
[24] Bergers L I J C, Hoefnagels J P M and Geers M G D 2014 On-wafer time-dependent high reproducibility nano-force tensile testing *J. Phys. D: Appl. Phys.* **47** 495306
[25] Gupta S and Pierron O N 2016 MEMS based nanomechanical testing method with independent electronic sensing of stress and strain *Extreme Mechanics Letters* **8** 167–76 (www.sciencedirect.com/science/article/pii/S2352431616000122)
[26] Kang W, Han J H and Saif M T A 2010 A novel method for in situ uniaxial tests at the micro/nanoscale-part II: Experiment *J. Microelectromech. Syst.* **19** 1322–30
[27] Kang W and Saif M T A 2010 A novel method for in situ uniaxial tests at the micro/nano scalepart-I: Theory *J. Microelectromech. Syst.* **19** 1309–21
[28] Komai K, Minoshima K and Inoue S 1998 Fracture and fatigue behavior of single crystal silicon microelements and nanoscopic AFM damage evaluation *Microsyst. Technol.* **5** 30–7
[29] Persson K and Boustedt K 2002 Fundamental requirements on mems packaging and reliability. 2002 Proc. 8th Int. Advanced Packaging Symp. pp 1–7
[30] Mercier D, Mandrillon V, Holtz A, Volpi F, Verdier M, and Bréchet Y 2012 Quantitative evolution of electrical contact

resistance between aluminum thin films. *2012 IEEE 58th Conf. on Electrical Contacts (Holm)* (September) pp 1–8
[31] Slade P G 2017 *Electrical Contacts: Principles and Applications* (Boca Raton, FL: CRC press)
[32] Diop M D, Mandrillon V, Boutry H, Inal K and Fortunier R 2010 Analysis of nickel cylindrical bump insertion into aluminium thin film for flip chip applications *Microelectron. Eng.* **87** 522–6 (www.sciencedirect.com/science/article/pii/S0167931709005139)
[33] Tan K K and Ng S C 2001 Computer controlled piezo micromanipulation system for biomedical applications *Eng. Sci. Educ. J.* **10** 249–56
[34] Greer J R and De Hosson J T M 2011 Plasticity in small-sized metallic systems: Intrinsic versus extrinsic size effect *Prog. Mater. Sci.* **56** 654–724
[35] Fleck N A and Hutchinson J W 1997 Strain gradient plasticity *Advances in Applied Mechanics* **33** 296–361
[36] Bergers L I J C, Hoefnagels J P M and Geers M G D 2014b On-wafer time-dependent high reproducibility nano-force tensile testing *J. Phys. D: Appl. Phys.* **47** 495306
[37] Ruybalid A P, Hoefnagels J P M, van der Sluis O and Geers M G D 2016 Comparison of the identification performance of conventional FEM updating and integrated DIC *Int. J. Numer. Methods Eng.* **106** 298–320
[38] van de Looij-Kleinendorst S M 2019 Image based mechanical characterization methods for stretchable electronic interconnects *PhD thesis* Department of Mechanical Engineering Technische Universiteit Eindhoven
[39] Bertin M, Chaowei D, Hoefnagels J P and Hild F 2016 Crystal plasticity parameter identification with 3d measurements and integrated digital image correlation *Acta Mater.* **116** 321–31 (www.sciencedirect.com/science/article/pii/S135964541630458X)
[40] Kleinendorst S M, Hoefnagels J P M, Fleerakkers R C, van Maris M P F H L, Cattarinuzzi E, Verhoosel C V and Geers M G D 2016 Adaptive isogeometric digital height correlation: Application to stretchable electronics *Strain* **52** 336–54
[41] Fleming A J and Leang K K 2014a *Design, Modeling and Control of Nanopositioning Systems* (Cham: Springer Int. Publishing)
[42] Fleming A J and Leang K K 2014b *Position Sensors* (Cham: Springer Int. Publishing) pp 103–53
[43] Coulombier M, Guisbiers G, Colla M-S, Vayrette R, Raskin J-P and Pardoen T 2012 On-chip stress relaxation testing method for freestanding thin film materials *Rev. Sci. Instrum.* **83** 105004
[44] Hemker K J and Sharpe W N 2007 Microscale characterization of mechanical properties *Annual Review of Materials Research* **37** 93–126
[45] Kang W, Merrill M and Wheeler J M 2017 In situ thermomechanical testing methods for micro/nano-scale materials *Nanoscale* **9** 2666–88